ISSN (Print) 1226-1750
ISSN (Online) 2233-6656
Journal of Magnetics 24(4), 641-649 (2019) https://doi.org/10.4283/JMAG.2019.24.4.641

Characteristics of Electric Motor according to the Weld-laminated Core and the Bond-laminated Core

Doo-Young Kim[1], Min-Ro Park[2], Young-Hoon Jung[2], Hyeon-Jin Park[2], Jung-Pyo Hong[2], and Myung-Seop Lim[2]*

[1]R&D Center, Hyundai Mobis, Yongin-si 16891, Republic of Korea
[2]Department of Automotive Engineering, Hanyang University, Seoul 133-791, Republic of Korea

(Received 3 January 2019, Received in final form 2 December 2019, Accepted 3 December 2019)

This paper examines the differences between the magnetic and mechanical characteristics of the motor core depending on the lamination method (weld and bond lamination) and analyzes the effects of these differences on the motor performance and vibration using analytical methods and tests. First, to analyze the magnetic and mechanical properties of iron cores according to lamination method, the initial magnetization curve and iron loss were measured, and the natural frequencies and damping ratios were identified through a modal test. Next, no-load and blocked-rotor tests of an induction motor were performed to determine the difference in the performance of the motor according to the lamination method. At this time, the loss occurring in the motor was divided into the primary copper loss, secondary copper loss, iron loss, and mechanical loss. Finally, the output, efficiency, and vibration of the motor were measured to analyze the effects of the magnetic and mechanical characteristics on the motor performance.

Keywords : electromagnetic forces, electric machines, lamination, vibration

1. Introduction

Today, electric motors are being used in various fields, such as in automobiles, household appliances, and industries, and the use of such motors is further increasing [1]. Among the existing electric motors, the permanent-magnet-type motor has been highlighted due to its advantages of high efficiency and high output. Due to the price fluctuations of the raw materials and the environmental issues of the permanent magnet, however, studies on motors that do not use permanent magnets have actively been conducted of late. The induction motor, which has been used and studied for a long time, has been highlighted again due to its low cost, easy operation, and relative eco-friendliness [2, 3]. As motors are used in a variety of fields, studies on their characteristics from various perspectives are in progress, and the manufacturing methods are also being diversified accordingly. In particular, as the use of electric motors for automobiles (e.g., for traction, EPS, and ISG), for household appliances (e.g., refrigerators, washing machines), and for elevators is closely related with everyday life, studies on the vibration and noise, which can be directly sensed by a user, are under way. The factors that affect the vibration and noise can be largely divided into magnetic, electronic, aerodynamic, and mechanical sources [4]. First, the magnetic source generates excitation force through the magnetic field that passes through the air-gap to create deformation in a stator, and if the frequency of this force matches the natural frequency, resonance occurs, and the sound vibrations are amplified. The studies on the vibration and noise created by the magnetic source are as follows. In [2, 5, 6], the vibration and noise were analyzed in accordance with the stator shape, pole angle, skew, overhang, and barrier of the rotor. In [7-10], the vibration orders by slot combination were compared, optimization for vibration and noise reduction was performed, and the unbalanced magnetic forces were analyzed according to the winding method used to compare and analyze the vibration and noise. As a result, these studies helped reduce the vibration and noise by controlling the spatial harmonics of the air-gap magnetic flux density in the motor design. Second, the vibration and noise caused by electronic sources occur as the input (including the

©The Korean Magnetics Society. All rights reserved.
*Corresponding author: Tel: +82-2-2220-4466
Fax: +82-2-2220-4467, e-mail: myungseop@hanyang.ac.kr

© 2019 Journal of Magnetics

harmonics) rather than the sinusoidal input is applied during the motor control. Especially, when the force generated by the harmonic input is generated near the natural frequency, the vibration and noise are further increased. In related studies [11], the vibration and noise were reduced through a method of avoiding the natural frequency of the stator by adjusting the magnitude and frequency of the PWM voltage. In [12, 13], harmonics were injected into the current to generate additional forces of the same magnitude and frequency as those that cause the vibration and noise in the opposite phase, thereby offsetting the two forces and reducing the vibration and noise. These studies helped reduce the vibration and noise through a method of controlling the motor. Third, the vibration and noise caused by the aerodynamic source occur due to the frequency of the coolant passing through the duct, vortex, and fan when the motor is cooled. Lastly, for the vibration and noise caused by a mechanical source, first, the rotor imbalance is one of their main causes. Such rotor imbalance not only causes the dynamic vibration of the rotor but also generates additional harmonics of the excitation force. Related to this study, the vibration and noise caused by the rotor imbalance due to the static and dynamic eccentricities of the rotor were investigated in [14]. The vibration and noise occur depending on the state of coupling between the load and the motor and between the motor and the support and depending on the bearing. One of the main factors for such is the mechanical property of the stator. As mentioned earlier, as resonance occurs if the frequency of the excitation force coincides with the natural frequency, the natural frequency of the stator is also important. Therefore, many studies have been conducted on the methods of calculating the natural frequency of the stator [15-18]. Most of these studies analyzed the vibration and noise for their design and control, but as mentioned earlier, the mechanical property of the stator is one of the main factors affecting the vibration and noise. Also, the stacking of the stator affects its mechanical characteristics [19, 20].

In this regard, this paper presents the differences in the electrical and mechanical characteristics depending on the stator lamination method during the manufacturing process of the motor and analyses the effects of such differences on the performance of the induction motor using analytical methods and tests. First, to compare the magnetic characteristics, the initial magnetization curve and iron loss of the stator core with two lamination methods were measured. Also, the frequency response function was confirmed through the modal test of the stator according to the lamination method, and the mechanical characteristics were analyzed by calculating the logarithmic decrement and the damping ratio as well as the natural frequency. Next, no-load, blocked-rotor, and load tests of the induction motor were performed to compare the performances of the motor according to the lamination method. The output power and efficiency of the motor were measured, and the primary copper loss, secondary copper loss, iron loss, and mechanical loss were separated from one another. Through the separation of the losses, the relationship between the changes in the magnetic characteristics according to the lamination method and the efficiency of the motor was analyzed. In addition, the deformation of the motor was measured, and the influence of the mechanical characteristics according to the lamination method on the vibration characteristics of the motor was presented.

2. Core Characteristics according to the Lamination Method

The core of the motor is made by laminating electrical steel sheets to reduce the eddy current loss, and as such, it becomes structurally weak in the lamination direction. Therefore, for structural stability, the weld and bond lamination methods are mainly used to laminate electrical steel sheets. The weld lamination method, the most

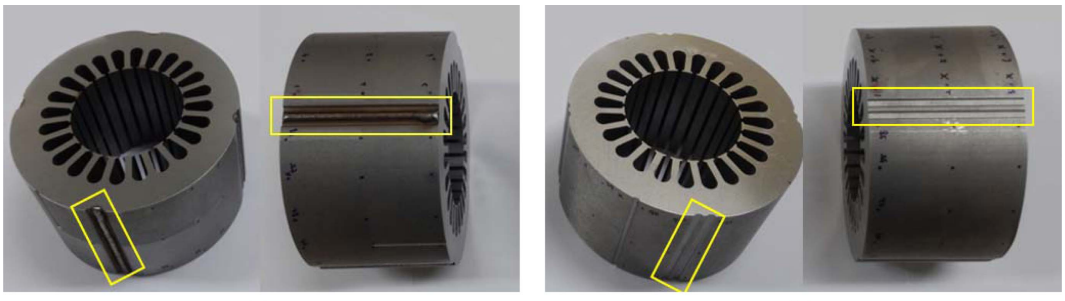

(a) (b)

Fig. 1. (Color online) Stator cores laminated using one of two lamination methods: (a) Weld-laminated stator core (b) Bond-laminated stator core.

commonly used lamination method, involves laminating electrical steel sheets and welding them under pressure. As for the bond lamination method, the bond is mixed in an about-0.5-micrometer-thick insulating material, is applied to the surface of the electrical steel sheets and is then laminated while applying heat and pressure to fix the sheets onto each other. Due to the differences in the adhesion between the electrical steel sheets and the deformation of the local materials caused by the heat and pressure applied for the lamination of the electrical steel sheets, the magnetic and mechanical characteristics of the core are changed. Therefore, for analysis purposes, a test was conducted to measure the magnetic and mechanical characteristics of the welded and bonded stator cores, as shown in Fig. 1. The electrical steel sheets that were used in the test were non-oriented ones, and the core of the weld lamination method was welded on the four sides at the same intervals.

2.1. Magnetic Characteristics

To compare the magnetic characteristics of the weld- and bond-laminated stator cores, a test was conducted to measure the initial magnetization curve and iron loss. Fig. 2 shows the test configuration; the primary and secondary windings were wound around the stator yoke in the circumferential direction [21]. The primary winding was connected to the AC voltage source and the magnetic flux density (B)-magnetic field intensity (H) analyzer, and the secondary winding was connected to the B-H analyzer. The devices that were used were the NF high-speed power amplifier and the IWATSU SY8258 B-H analyzer.

2.1.1. Initial magnetization curve

The initial magnetization curve, which is referred to as the B-H curve, exhibits DC magnetization characteristics.

$$B = \mu_0(1+\chi_m)H \tag{1}$$

Equation (1) represents the magnetization curve according to the magnetomotive force, where μ_0 is the magnetic

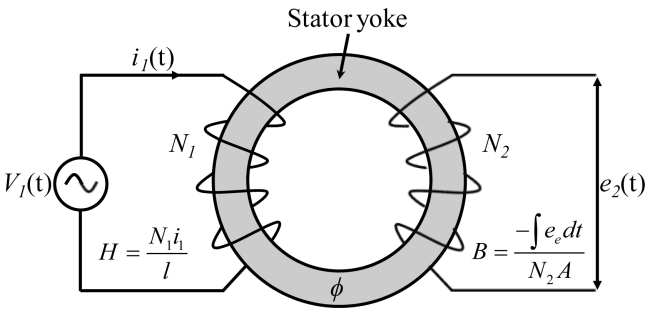

Fig. 2. (Color online) Test configuration for the magnetic characteristics.

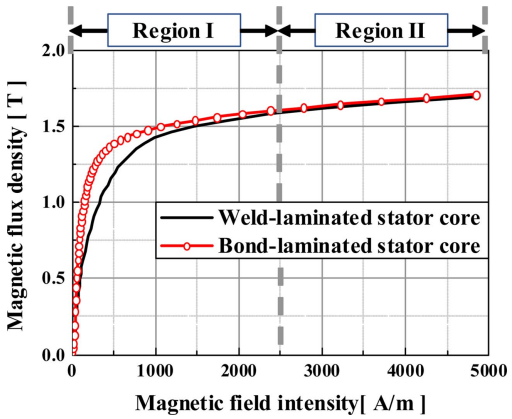

Fig. 3. (Color online) Initial magnetization curve.

permeability of a vacuum, and χ_m is the magnetic susceptibility that indicates the magnetic characteristics of the magnetic materials.

The test configuration was made from 0.1 to 1.7 T when the applied magnetomotive force ranged from 29.1 to 4845.6 A/m. Fig. 3 shows the initial magnetization curve measured from the welding and bending cores, respectively. In Fig. 3, the section was divided into Region I and II based on 50 % of the measured magnetomotive force range. In Region I, the magnetic flux density of the bond-laminated stator core was up to 57 % higher than that of the weld-laminated stator core, and 13 % higher on average. The saturated Region II, however, showed a magnetic flux density difference of about 1 % against the same magnetomotive force. The initial magnetization curve of the stator core according to the lamination method is determined by the manufacturing process. During the welding lamination process, the mechanical and thermal stresses on the electrical steel sheet deteriorate the magnetic properties of the stator core [22, 23]. In particular, the deterioration of the magnetic properties becomes more severe in the weld joint. However, the bonding laminations are coated with an adhesive varnish and laminated together during the thermal activation process [24]. At this time, the temperature of the thermal activation process is not high enough to affect the magnetic properties of the electrical steel sheet. Therefore, the B-H characteristic of the weld-laminated stator core is lower than the B-H characteristic of the bond-laminated stator core. Also, this degradation is worse than 1.5T [24, 25].

2.1.2. Iron loss

Iron loss occurs when a time-varying magnetic field is applied to a magnetic material. As mentioned earlier, as the magnetic characteristics of the electrical steel sheets

change during the lamination process, the iron loss also varies depending on the lamination method.

The electric motor is fabricated by laminating electrical steel sheets to reduce the eddy current loss of the magnetic core. However, when electrical steel sheets are weld-laminated, the weld joints of each sheet are connected through the bead. Thus, short circuits between each electrical steel sheet are created and eddy current loss increases [23]. In addition, through the Steinmetz's equation (2), the eddy current loss is proportional to the square of the frequency. Therefore, the higher the frequency, the greater the influence of the eddy current.

$$W_c = k_h B^2 f + k_e B^2 f^2 + k_a B^{1.5} f^{1.5} \quad (2)$$

where, k_h, k_e, k_a is hysteresis loss coefficient, eddy current coefficient, anomalous loss coefficient, respectively. B is magnetic flux density and f is frequency.

In accordance with the IEC 60404-2 standard, iron loss according to lamination method was measured up to 1.5T at 60 Hz and 0.8T at 400 Hz. Fig. 4 shows the measured iron losses of the weld- and bond-laminated stator core. To account for this, the measured iron losses are divided by (2) into hysteresis loss, eddy current loss and anomalous loss, respectively. As a result, as shown in Fig. 5, the rate of eddy current loss increases with increasing frequency. Therefore, at low frequencies where the rate of eddy current loss is low, the iron loss of the weld-laminated core is lower than that of the bond-laminated core. However, as the frequency increases, the rate of eddy current loss increases and the loss of weld-laminated core increases.

2.2. Mechanical Characteristics

Natural frequencies are affected by the mass and stiffness. To compare the mechanical characteristics of the weld- and bond-laminated stator cores according to the lamination method, the modal test was performed with cores that had the same shape, as in Fig. 1. Fig. 6 shows the modal-test configuration. The test was conducted using a roving impact hammer testing method, in which the accelerometer was attached to the stator, and the frequency response function (FRF) was measured at the impact position. The impact was applied to a total of 60 points, including 12 points in the circumferential direction and 5 in the axial direction, to measure the FRF. Equation (3) represents the natural frequencies.

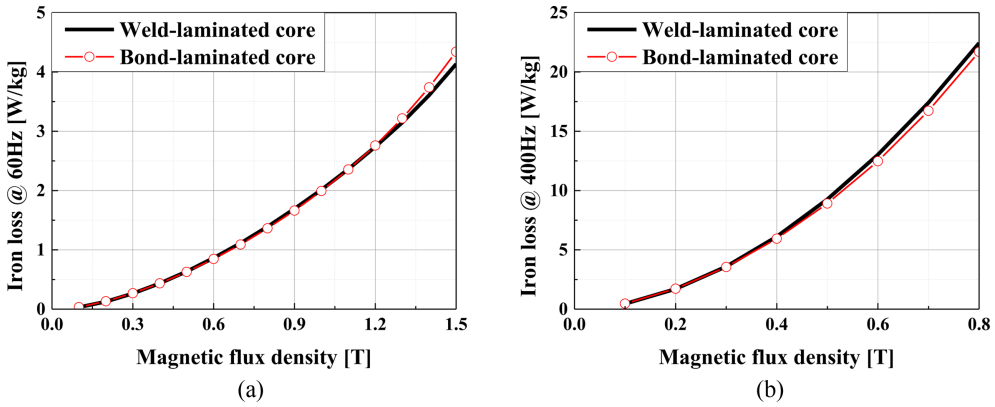

Fig. 4. (Color online) Iron loss (a) 60 Hz, (b) 400 Hz.

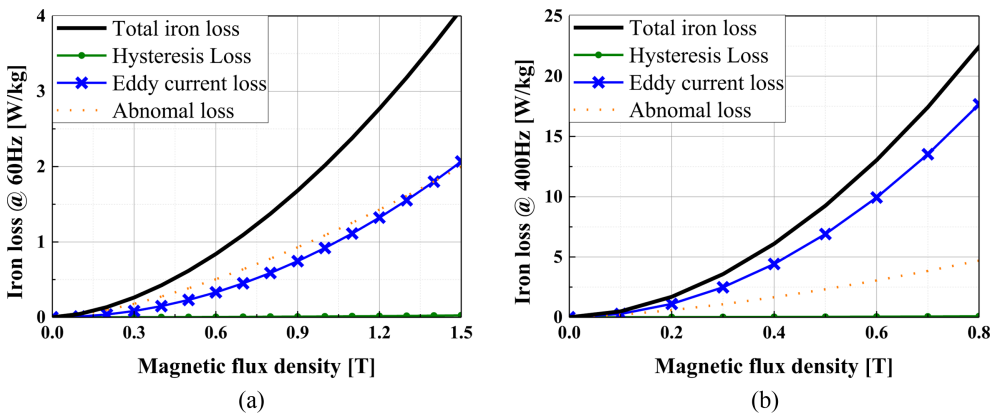

Fig. 5. (Color online) Iron loss rate of weld-laminated core (a) 60 Hz, (b) 400 Hz.

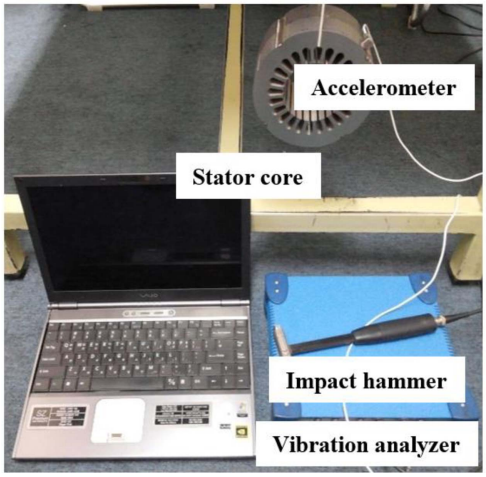

Fig. 6. (Color online) Set-up for the modal test.

$$f_n = \frac{1}{2\pi}\sqrt{\frac{K}{m}} \tag{3}$$

where m is the mass of the object and K is the stiffness that indicates the resistance of the deformation to the load acting on the object.

The damping ratio is an indicator of how much the vibration of an object that vibrates in a specific form is reduced or attenuated depending on its cycle and is dependent on the frequency and mode shape. It is calculated by obtaining the logarithmic decrement experimentally. Equation (4) represents the logarithmic decrement, and the relationship between the damping ratio and the logarithmic decrement is shown in (5).

$$\delta = \frac{\pi f_{delta}}{f_n} \tag{4}$$

$$\zeta = \frac{1}{\sqrt{1+(\pi/\delta)^2}} \tag{5}$$

where f_n is the natural frequency, f_{delta} is the frequency width that corresponds to 0.707 times the peak displacement at f_n, and ζ is the damping ratio. Fig. 7 shows the FRF characteristics of the stator core obtained from the modal test according to the lamination method. The FRF characteristics of up to 7000 Hz was measured in the test as shown in Fig. 7. The natural frequency, stiffness, and damping ratio of each stator core in circumferential 2 mode shape were calculated using the measured FRF and equations (3), (4), and (5), and the calculated parameters are shown in Table 1. As shown in the FRF graph in Fig. 7, the change in the natural frequencies of circumferential mode shapes 2 depending on the lamination method is less than 1 %, which means that the difference in the stiffness of circumferential mode shapes 2 is less than 1 % according to the lamination method. As shown in Table 1, the difference in stiffness between circumferential mode shapes 2 of the core is less than 1 % depending on the lamination method. The damping ratio for circumferential mode shapes 2, however, was 87.74 % in the bond-laminated stator core, showing a 43.84 % increase. This means that there was no difference in the response to the static force between the two lamination methods, but the displacement response to the dynamic force is smaller in the bond-laminated stator core than in the weld-laminated stator core. The next chapter examines the effects of the differences in the magnetic and mechanical characteristics of the core on the characteristics of the motor according to the lamination method.

3. Confirmation through Experiments

The effects of the magnetic and mechanical characteristics on the actual motor driving according to the lamination method and examined in section 2 were confirmed by

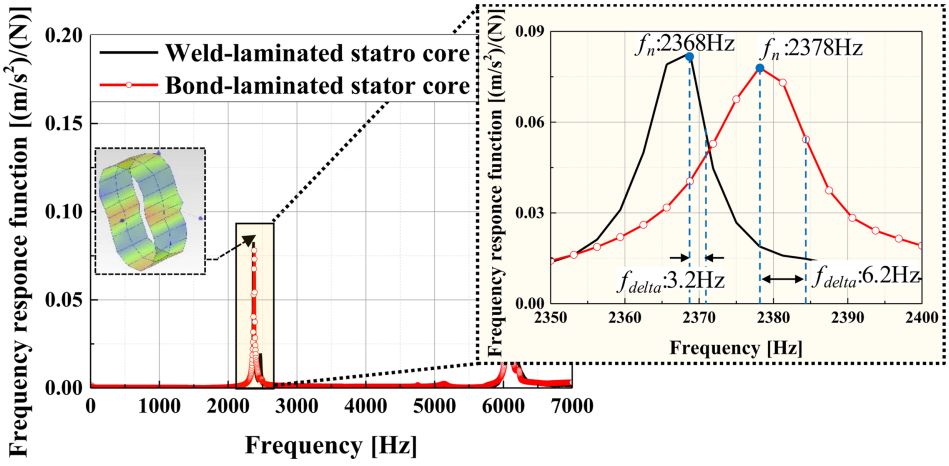

Fig. 7. (Color online) Frequency response function.

Table 1. Modal analysis

	Circumferential mode shape	Weld-laminated	Bond-laminated	Difference [%]
Natural frequency [Hz]	Mode shape 2	2368	2378	0.42
Stiffness [N/m]	Mode shape 2	1122.92	1125.38	0.22
Damping ratio [-]	Mode shape 2	0.001395	0.002619	87.74

using 1.5 kW, two-pole, 31/24 (rotor/stator) squirrel cage induction motors. Load and loss separation tests were performed to investigate the effects of the differences in the magnetization characteristics according to the two lamination methods. The loss in the motor is largely divided into copper loss, iron loss, and mechanical loss. The parameters of the motor equivalent circuit were calculated through the no-load and blocked-rotor tests for measuring the load iron and copper losses on the secondary side in the squirrel cage induction motor. The mechanical and copper losses on the primary side were measured through the test. The effects of the lamination methods on the mechanical characteristics were confirmed by the vibration test.

3.1. Load Test

The test compared the line-to-line voltage, current, torque, and efficiency of the motors made with the two different lamination methods at 4 Nm and 3500 rpm. As shown in Table 2, the motor using the bond-laminated stator core exhibited 1.34 % higher efficiency. The bond-laminated motor uses 0.92 % less current, and this is because the bond-laminated stator core has good BH characteristics, as shown in section 2.

3.2. Loss Separation from the No-Load and Blocked-Rotor Tests

The primary copper loss, secondary copper loss, and iron loss were calculated using the equivalent circuit shown in Fig. 8. The parameters of the equivalent circuit were obtained through the no-load and blocked-rotor tests. Table III shows the active power, reactive power, input current, and phase resistance on the primary side for the no-load and blocked-rotor tests. Generally, in the no-load test, the secondary-side circuit is open, and the equivalent circuit ignores the excitation current in the blocked-rotor test. In this paper, however, the resistance on the secondary side (r'_2), the leakage reactance on the primary (x_1) and secondary sides (x'_2), the iron loss resistance (r_c), and the magnetization reactance (x_m) were calculated using equations (6), (7), (8), (9), and (10) as well as the equivalent circuit in Fig. 8 that does not ignore the excitation current in the blocked-rotor test.

Table 2. Load test

	Weld-laminated motor	Bond-laminated motor
Line-line voltage [Vrms]	380	380
Current [Arms]/Frequency [Hz]	3.25/60	3.22/60
Torque [Nm]	4.01	4.02
Speed [rpm]	3501	3510
Efficiency [%]	83.90	85.24

$$P_N = R_{Neq} I_N^2 = I_N^2 \times \left(r_1 + \frac{r_c x_m^2}{r_c^2 + x_m^2} \right) \tag{6}$$

$$Q_N = X_{Neq} I_N^2 = I_N^2 \times \left(x_1 + \frac{r_c^2 x_m}{r_c^2 + x_m^2} \right) \tag{7}$$

where P_N is the active power under the no-load test, Q_N is the reactive power under the no-load test, I_N is the input current under the no-load test, R_{Neq} is the real part of the no-load equivalent impedance, and X_{Neq} is the imaginary part of the no-load equivalent impedance.

$$P_B = R_{Beq} I_B^2 = I_B^2 \times \left(r_1 + \frac{r_c x_m x'_2 (x_m x'_2 - r_c r'_2) + r_c r'_2 x_m (r_c x_m + r_c x'_2 + r'_2 x_m)}{(r_c r'_2 - x_m x'_2)^2 + (r_c x_m + r_c x'_2 + r'_2 x_m)^2} \right) \tag{8}$$

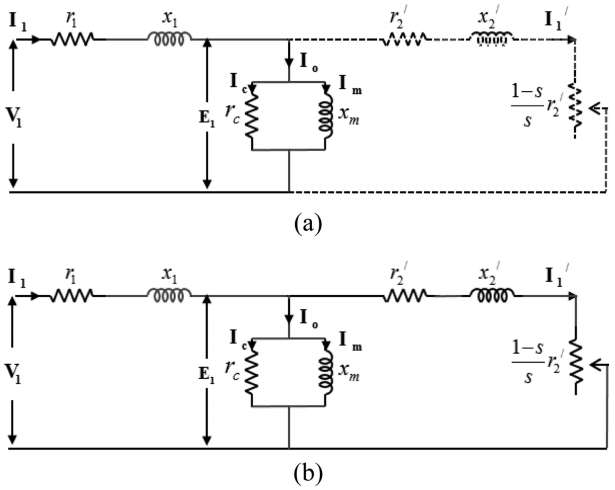

Fig. 8. Equivalent circuit (a) No-load test, (b) Blocked-rotor test.

$$Q_B = X_{Beq} I_B^2 = I_B^2 \times \left(x_1 + \frac{r_c x_m x_2' (r_c x_m + r_c x_2' + r_2' x_m) + r_c r_2' x_m (r_c r_2' - x_m x_2')}{(r_c r_2' - x_m x_2')^2 + (r_c x_m + r_c x_2' + r_2' x_m)^2} \right) \quad (9)$$

$$x_1 = x_2' \quad (10)$$

where P_B is the active power under the blocked-rotor test, Q_B is the reactive power under the blocked-rotor test, I_B is the input current under the blocked-rotor test, R_{Beq} is the real part of the blocked-rotor equivalent impedance, and X_{Beq} is the imaginary part of the blocked-rotor equivalent impedance. The ratio of the leakage reactance on the primary side to the leakage reactance on the secondary side of (10) is 1:1, because the motor to be tested was a NEMA-class-A-type motor. Table 3 shows the active power, reactive power, phase voltage, current, and primary-side resistance measured in the no-load and blocked-rotor tests. The blocked-rotor test is proceeded at 25 % of the rated frequency to consider the magnetic saturation and the skin effect when driving at the rated voltage. Based on the values obtained from the measurement, five parameters were calculated by combining Equations (6)-(10). These parameters are shown in Table 4. The parameters of the equivalent circuit were analyzed under the no-load test conditions to obtain the copper loss on the primary and secondary sides and the iron loss, and the mechanical loss was measured at 3500 rpm through the test. Fig. 9 shows the loss proportions of the weld- and bond-laminated motors. The differences in losses between the two lamination methods were 1.41 % for the copper loss on the primary side and 0.44 % for the copper loss on the secondary side. The iron loss showed a 9.60 % increase in the bond-laminated motor, however, and this is because the iron loss per unit weight at a 60 Hz power frequency was increased in the section where the magnetic flux density of the bond-laminated stator core was more than 1.2 T.

Table 3. No-load and blocked-rotor tests

		Weld-laminated motor	Bond-laminated motor
Effective power [W]	No-load test	28.00	35.43
	Blocked-rotor test	50.93	55.10
Reactive power [var]	No-load test	360.10	373.27
	Blocked-rotor test	23.27	23.57
Input current [Arms]	No-load test	1.65	1.70
	Blocked-rotor test	3.22	3.28
Primary-phase Resistance (r_1) [Ω]	No-load test Blocked-rotor test	3.22	3.26

Table 4. The parameters of equivalent circuit

	Weld-laminated motor	Bond-laminated motor
r_2'	1.72	1.99
x_2'	4.41	4.22
x_1	4.41	4.22
r_c	1897.93	1737.89
x_m	125.79	125.02

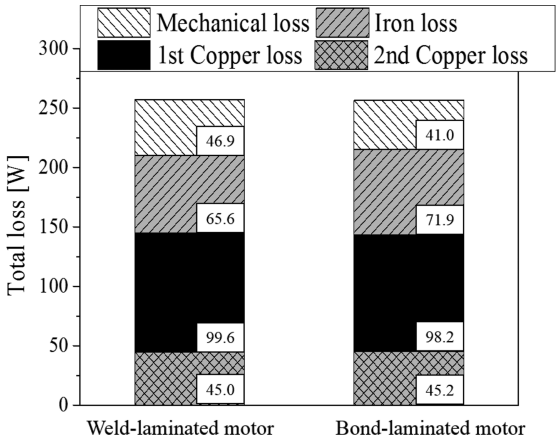

Fig. 9. Loss segregation.

3.3. Vibration Test

Prior to the vibration test, the radial electromagnetic force caused by the variation of magnetic characteristics according to the weld-lamination and bond-lamination was calculated using finite-element analysis (FEA). Fig. 10 shows the radial electromagnetic forces applied to the stator cores according to the lamination method. As explained in section 2, the magnetic flux density was 13 % higher on average in Region I for the bond-laminated core under the condition of the same magnetomotive force, but the difference is about 1 % in Region II. The radial magnetic force, however, is almost not influenced by this difference because the magnetic resistance in the air-gap is dominant. Therefore, since these forces according to lamination methods are nearly similar, the waveforms of the two forces overlap as shown in Fig. 10 (a). Also, as shown in Fig. 10 (b), the results of the harmonic analysis of the two forces are almost identical.

The vibration tests of the motors using two different lamination methods were conducted under the same load conditions at 4 Nm and 3500 rpm. The accelerometer was attached to the position shown in Fig. 11, and the motor vibrations depending on the lamination method were compared. Fig. 12 (a) shows the vibrations according to the frequencies. To evaluate the overall vibration, the total vibration was calculated, as shown in (11).

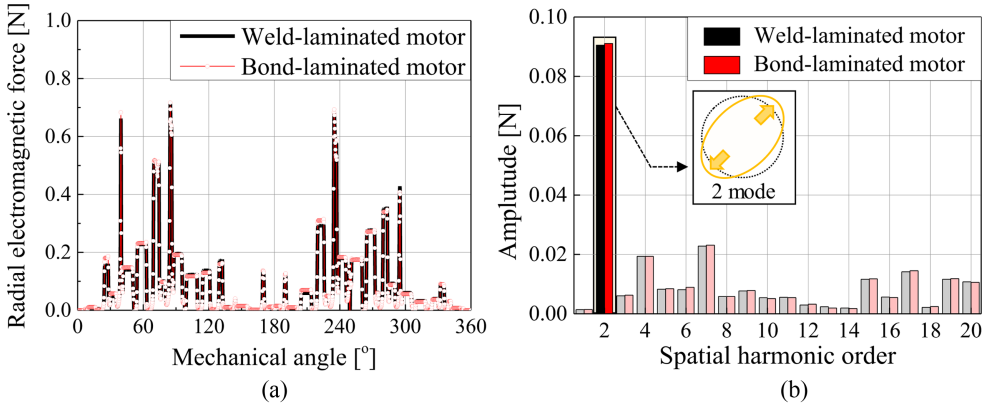

Fig. 10. (Color online) Radial electromagnetic force (a) Waveform, (b) Harmonic analysis.

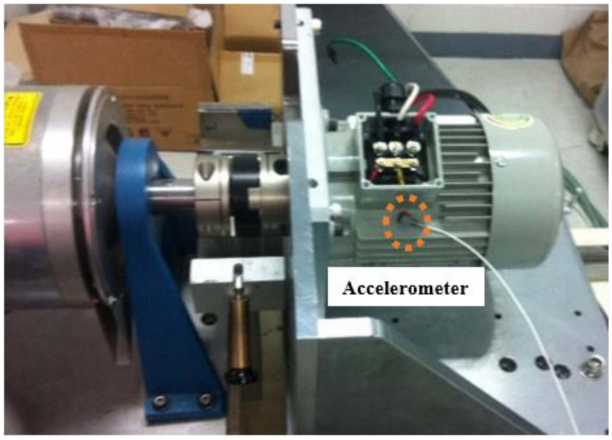

Fig. 11. (Color online) Set-up for the vibration test.

$$L_a = 10\log\sum\left(\frac{a_i^2}{a_0^2}\right) \tag{11}$$

where a_i is the magnitude of the i-th order harmonic acceleration, and a_0 is the reference value with $a_0 = 1 \times 10^{-6}$ m/s^2. The overall vibration within 2000 Hz was 125.7 dB for the weld-laminated motor and 123.2 dB for the bond-laminated motor, showing a 2.5 dB reduction in the bond-laminated motor. As the target motor has two poles, the spatial harmonic order of the main electromagnetic force that causes the vibration of the frequency component is 2 as shown in Fig. 10 (b) [26]. In addition, the radial electromagnetic force was almost unchanged according to the lamination method as shown in Fig 10. At this time, the mechanical dynamic equation is as shown in (12).

$$\frac{d^2x(t)}{dt^2} + 2\zeta\omega_n\frac{dx(t)}{dt} + \omega_n^2 x(t) = \frac{F(t)}{M} \tag{12}$$

where, x is the displacement, F is the force, M is the mass, ζ is the damping ratio and ω_n is the undamped natural frequency.

As shown in Table 1, in circumferential mode shape 2, the natural frequency and damping ratio of bond-laminated motors increased by 0.42 % and 87.74 %, respectively. Therefore, as can be seen from (12), the vibration of bond-laminated motor is reduced than vibration of weld-laminated motor for the same force/mass. Therefore,

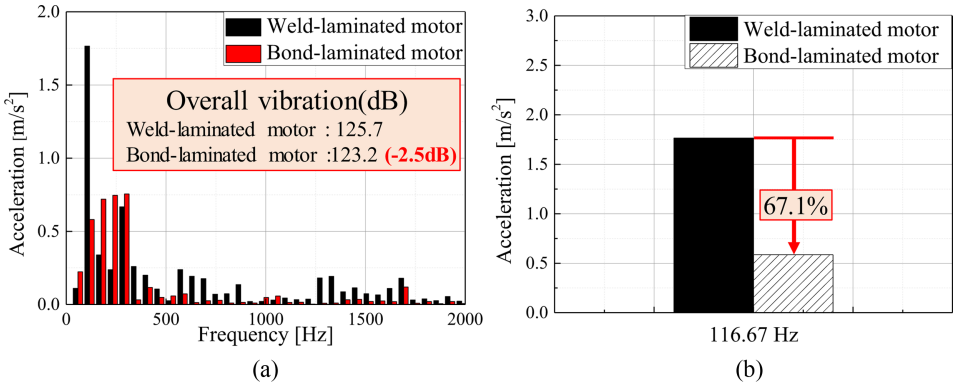

Fig. 12. (Color online) Comparison of the vibrations of the weld- and bond-laminated motors: (a) Total vibration comparison, (b) Comparison of the vibration at the frequencies with two times the rotational speed.

when driven under the same load conditions, the overall vibration is superior to bond-laminated motor.

Especially, the vibration of the frequency component with two times the rotational speed is dominantly affected by the damping and stiffness of mode shape 2. Therefore, as shown in Fig. 12 (b), the vibration of the bond-laminated motor was reduced by 67.11 % at 116.67 Hz, which corresponds to two times the rotational speed. That is because the damping ratio of circumferential mode shape 2 is increased by 87.74 % compared to the weld-laminated motor.

4. Conclusion

This paper discusses the differences in the magnetic and mechanical characteristics of electrical steel sheets depending on two lamination methods: weld lamination and bond lamination. First, the BH characteristics and iron loss were measured through the stator cores laminated using the two aforementioned methods to confirm the difference in the magnetic characteristics, and the difference in the mechanical characteristics was examined through the modal test. Based on the results, bond lamination showed better BH characteristics than weld lamination, and the iron loss was increased at 60 Hz. In addition, the difference in the natural frequencies of the weld- and bond-laminated stator cores was less than 1 %, but the damping ratio showed an 87.74 % increase in the bond-laminated stator core based on mode shape 2. Therefore, it can be said that bond lamination has characteristics that are more advantageous to the vibration compared to weld lamination. Further, the characteristics examined through the load test were verified by applying the two lamination methods to the actual motor. In conclusion, this paper shows the differences in the magnetic and mechanical characteristics of the core according to the lamination method. The findings of this paper are expected to help in the selection of the lamination method to be used in the motor for applications where the vibration is important.

Acknowledgment

This work was supported by the National Research Foundation of Korea(NRF) grant funded by the Korea government(MSIP; Ministry of Science, ICT & Future Planning) (No. 2018R1C1B5085447).

References

[1] M. R. Park, H. J. Kim, Y. Y. Choi, J. P. Hong, and J. J. Lee, IEEE Trans. Magn. **52**, 1 (2016).
[2] J. W. Jung, S. H. Lee, G. H. Lee, J. P. Hong, D. H. Lee, and K. N. Kim, IEEE Trans. Magn. **46**, 2454 (2010).
[3] D. J. Kim, H. J. Kim, J. P. Hong, and C. J. Park, IEEE Trans. Magn. **50**, 857 (2014).
[4] P. Vijayraghavan and R. Krishnan, IEEE Trans. Ind. Appl. **35**, 1007 (1999).
[5] J. W. Jung, D. J. Kim, J. P. Hong, G. H. Lee, and S. M. Jeon, IEEE Trans. Magn. **47**, 3661 (2011).
[6] Cassat, A. *et al*., IEEE Trans. Ind. Appl. **48**, 1526 (2012).
[7] Z. Q. Zhu, Z. P. Xia, L. J. Wu, and G. W. Jewell, IEEE Trans. Ind. Appl. **46**, 1908 (2010).
[8] G. Verez, G. Barakat, Y. Amara, and G. Hoblos, IEEE Trans. Magn. **51**, 1 (2015).
[9] Z. Q. Zhu, Z. P. Xia, L. J. Wu, and G. W. Jewell, in Proc. Energy Convers. Congr. Expo. (ECCE), 3443 (2009).
[10] S. Zuo, F. Lin, and X. Wu, IEEE Trans. Ind. Electron. **62**, 6204 (2015).
[11] H. Stemmler and T. Eilinger, in Proc. IEEE PESC'94, **1**, 269 (1994).
[12] D. Torregrossa, D. Paire, F. Peyraut, B. Fahimi, and A. Miraoui, IEEE Trans. Ind. Electron. **59**, 1346 (2012).
[13] D. Belkhayat, D. Roger, and J. F. Brudny, in Proc. 8th Int. Conf. Electrical Machines and Drives, 400 (1997).
[14] D. G. Dorrell, W. T. Thomson, and S. Roach, IEEE Trans. Ind. Appl. **33**, 24 (1997).
[15] A. J. Ellison, and S. J. Yang, in Proc. Inst. Elect. Eng. **118**, 185 (1971).
[16] D. E. Cameron, J. H. Lang, and S. D. Umans, IEEE Trans. Ind. Appl. **28**, 1250 (1992).
[17] W. Cai, P. Pillay, and Z. Tang, IEEE Trans. Ind. Appl. **38**, 1027 (2002).
[18] R. Islam, and I. Husain, IEEE Trans. Ind. Appl. **46**, 2346 (2010).
[19] Z. Tang, P. Pillay, A. M. Omekanda, C. Li, and C. Cetinkaya, IEEE Trans. Ind. Appl. **40**, 748 (2004).
[20] Y. Gao, K. Muramatsu, M. J. Hatim, and M. Nagata, IEEE Trans. Magn., **47**, 1358 (2011).
[21] D. Kim, J. Chin, J. Hong and M. Lim, IET Electric Power Appl. **13**, 1280 (2019).
[22] J. Kim, PhD Thesis, Automotive Engineering. Hanyang university, Seoul, Korea (2016).
[23] Krings, A., PhD Thesis, KTH Royal Inst. Tech., Stockholm, Sweden (2014).
[24] A. Schoppa, J. Schneider, C. D. Wuppermann, and T. Bakon, J. Magn. Magn. Mater. **254-255**, 367 (2003).
[25] A. Schoppa, J. Schneider and C.D. Wuppermann, J. Magn. Magn. Mater. **215-216**, 74 (2003).
[26] M. Park, J. Jung, D. Kim, J. Hong, and M. Lim, IEEE Trans. Ind. Appl. **55**, 1351 (2019).